(200)
R290

Lithograph also published version ... U.S. Geological Survey ... report NASA-139

69-27

UNITED STATES

DEPARTMENT OF THE INTERIOR

GEOLOGICAL SURVEY

POST-EARTHQUAKE INFRARED IMAGERY, PARKFIELD-CHOLAME, CALIFORNIA EARTHQUAKES OF JUNE—AUGUST, 1966

by

Robert D. Brown, Jr.

1969

U.S. Geological Survey
OPEN FILE REPORT

This report is preliminary and has not been edited or reviewed for conformity with Geological Survey standards or nonenclature.

CONTENTS

List of illustrations

Figure 4B. Midday (about 1200 Pacific Daylight Time 7-28-66) Reconofax IV infrared imagery of northern Cholame Valley and vicinity. Arrow indicates approximate north. Double arrows indicate approximate range of incidence of sun's rays during overflight.

4C. Panchromatic vertical aerial photo of a part of the area shown in figs. 4A and 4B.

5A. Early morning about 0600 Pacific Daylight Time 7-29-66) Reconofax IV infrared imagery of Parkfield-Middle Mountain area. Arrow indicates approximate north.

5B. Midday (about 1200 Pacific Daylight Time 7-28-66) Reconofax IV infrared imagery of Parkfield-Middle Mountain area. Arrow indicates approximate north. Double arrows indicate approximate range of incidence of the sun's rays during overflight.

5C. Panchromatic vertical aerial photo of a part of the area shown in figs 5A and 5B.

6. Generalized geologic map of the Parkfield-Cholame area, modified from Jennings (1958), Marsh (1960), Dickinson (1963, 1966a,b) and unpublished maps by T. W. Dibblee, Jr.; (1967, fig. 3).

Figure 7. Sketch map of test area near Gold Hill, site of ground temperature observations of 7-29-68 and 7-30-68.

8. Comparison of soil and air temperature records from ground test area near Gold Hill.

9. Comparison of infrared temperature for bare soil, dry grass, and green vegetation at test area near Gold Hill

10. Comparison of air temperature and humidity in green vegetation and over dry-grass covered area at test area near Gold Hill.

TABLE

I. Comparison of U. S. Weather Bureau air temperature in °Centigrade for July 28-29, 1966 and July 29-30, 1968.

Introduction

This report concerns infrared imagery obtained over an active segment of the San Andreas fault during a period of continuing earthquake shocks and measurable fault displacement. The investigation described is part of a U.S. Geological Survey program to test and evaluate geologic applications of a number of recently developed remote sensor techniques in use by the National Aeronautics and Space Administration. It was undertaken to determine whether detectable thermal anomalies, marked by 8-13μ infrared radiation, accompany active faulting.

Despite generally favorable conditions and high-quality imagery, no anomalies of the type sought were detected. However, the imagery does illustrate very clearly a number of features that help locate the San Andreas fault, and it shows both the limitations and advantage of this remote sensing device. This report describes the geologic conditions under which the imagery was obtained, the kinds of thermal anomalies that were sought, and the results shown by the imagery. It also briefly examines some vegetation contrasts that are thought to be responsible for some of the fault-line anomalies evident in the imagery.

The San Andreas fault is a major tectonic feature with right-lateral strike separation measurable in scores of miles. Its current and historic activity is shown by numerous earthquakes and by many examples of fault movement at the earth's surface. Because of its tectonic importance, its 600-mile length, and its ready accessibility it has been used to evaluate and test a number of remote sensing techniques. For example, Wallace and Moxham (1966) discussed empirical relations observed in infrared imagery along a segment of the

San Andreas fault in the Carrizo Plain and Brown (1966), in another empirical study, related side-looking radar imagery to geology. Other studies utilizing remote sensing techniques are in progress along selected parts of the San Andreas fault. Of necessity most of these investigations must deal indirectly with the measurable geologic effects of past faulting rather than directly with the process of faulting. This is fortunate in some respects, for the geologic effects of numerous episodes of fault movement tend to be cumulative. They thereby magnify or enhance evidence of tectonic activity that might not be apparent after a single episode of fault movement. On the other hand, it is often useful to study dynamic geologic processes when they are in operation, as Fischer and others (1964) have done with infrared surveys of Hawaiian volcanoes.

An opportunity to investigate an episode of fault movement on the San Andreas fault was afforded by the Parkfield-Cholame earthquakes of June-August 1966. The location of this area is shown in figure 1. This earthquake sequence began on June 27 with 2 foreshocks that preceded the main shock of 5.5 magnitude at 9:26 p.m. Pacific Daylight Time. The earthquakes--and the aftershocks that continued for several months--were accompanied by surface tectonic fractures that exhibited several inches of right-lateral strike slip displacement. Fault rupture at the surface was mapped for 23 miles and was observed both on the main trace of the San Andreas fault and on a subsidiary trace about 0.7 mile southwest of the main fault. The strike-slip displacement was monitored by a series of strain-measuring quadrilaterals and detectable movement was recorded for more than a month after the main shock on June 27. These and other

observations on the fault movements and earthquake activity are recorded in detail elsewhere (Brown and others, 1967).

The extended duration of earthquake activity and fault movements between Parkfield and Cholame provided ideal conditions to study these phenomena with a variety of geologic and geophysical tools. Infrared surveys of the faulted area were undertaken because it seemed possible that surface thermal anomalies might be formed as a result of the fault activity. For example, under favorable conditions thermal anomalies might be formed by:

a. Above normal heat-flow associated directly with the process of faulting and with the movement of one fault block past another.

b. Disruption of the ground-water system by faulting in such a way that the pre-earthquake water-table is substantially elevated or lowered with respect to the ground surface.

c. Introduction of warmer waters, from deep confined aquifers, into the near-surface ground-water supply, or the more easily detected--

d. Introduction of warmer waters into surface streams.

e. Abnormal cooling (due to greater surface exposure) of mole-tracked and fractured ground that is one surface expression of faulting.

Anomalies arising solely from (a) above are unlikely to be detectable by the infrared surveys described here. In a study of the heat flow across the San Andreas fault further north Brune and Roy (1968) suggest that any heat-flow anomaly due to friction on the fault is less than

0.2μ cal/cm^2 sec and they cite heat flow values of 1.2μ cal/cm^2 sec for a line of heat flow stations that cross the fault near Hollister, California. At the surface of the earth, absorption and reflection of solar heat, and radiation of thermal energy into the atmosphere cause daily fluctuations in surface temperatures that are orders of magnitude greater than the contribution of geothermal heat. Consequently, precise studies of geothermal flux are commonly made in bore-holes or mines to reduce or eliminate the effects of surface heating. Because the heat flow associated with fault movements is even less than that normally measured in studies of the geothermal gradient, it is not surprising that no such anomaly was detected.

Temperature differences of several degrees centigrade are commonly encountered as a result of near-surface water tables and such differences are detectable with the infrared imaging systems used. Many of the most evident anomalies on both daytime and nighttime infrared imagery can be related to the presence of water--in the ground, ponded, or in flowing streams or possibly to the effects of soil moisture as postulated by Wallace and Moxham (1966).

In addition to the anomalies that might be associated with active fault movements, some geologic units are known to display characteristic infrared signatures due to their own peculiar chemical or physical properties. Such units are most easily recognized and delineated where vegetation is sparse and soil cover is thin. Although the area described here is not one of heavy or dense vegetation, most of it has some form of vegetative cover and alluvium and soil commonly extend to depths of at least several feet along the fault. The area, therefore, is not

well suited to the study of the infrared radiation characteristics of bedrock units, but it does offer the possibility of detecting subtle soil, ground water, or geologic differences that are reflected in vegetation patterns, for vegetation of different types and in different stages of life are detectable by infrared surveillance.

Infrared imagery

Several sets of infrared imagery are available for the segment of the San Andreas fault between Parkfield and Cholame. A daylight strip obtained on June 4, 1965 and at about 1:80,000 scale is part of an extensive infrared survey of the San Andreas fault in the central Coast Ranges that was made using a Reconofax III system in a NASA aircraft. Although the imagery for this strip is high quality, it shows chiefly the effects of mid-day solar heating, which do not facilitate geologic interpretation. It does, however, show a number of features along the San Andreas fault, and in some places the fault can be accurately delineated on the basis of the imagery. It is of interest here only because it forms some basis for comparison with post-earthquake infrared daytime imagery.

The first post-earthquake infrared imagery was obtained during daylight hours on July 7, 1966 using a Bendix infrared imaging radiometer aboard an Abrams Aerial Survey Corp. aircraft. This imagery, at a scale of about 1:13,000, lacks the sharp contrast and fine detail that was achieved subsequently with the Reconofax IV system, but it portrays adequately the more evident daytime thermal anomalies. For most of the areas imaged the detail is adequate for accurate location of geographic points, and the infrared signature patterns clearly show: trees, tanks,

springs, seeps, stream courses, roads (both paved and unpaved), cattle trails, buried pipelines, and fields in various stages of cultivation. Parts of the San Andreas fault can be identified from the infrared signatures of sag depressions, offset streams, and straight stream courses, but it is generally difficult to locate the fault solely on the basis of the imagery. Like the June 1965 imagery, that obtained with the Bendix instrument is not ideally suited to geologic interpretation because it was obtained during daylight hours. Several nighttime overflights were made with the Bendix system, but apparently instrumental difficulties were not overcome and no usable nighttime imagery was obtained.

On July 28 and 29, 1966 additional infrared imagery was obtained along the fault trace by a NASA Convair 240A equipped with a Reconofax IV infrared scanning system. These flights were planned to gather 2 sets of infrared data: one during the daylight hours, the other just before sunrise. Of the two, the pre-sunrise flight was the most important for geologic interpretation. Just before daylight solar heating effects are minimized, most radiating surfaces have lost a large part of the infrared energy absorbed during the daylight hours, and consequently differences in radiation patterns that are due to geologic phenomena become relatively more detectable.

The daytime flight was completed between 12:36 and 1:05 p.m. Pacific Daylight Time, on July 28. The early morning flight on July 29 encountered aircraft positioning problems due to poor visibility. This resulted in some delay so that the sun had risen before the flight was completed. Imagery was obtained between 5:43 and 6:07 a.m. (Pacific Daylight Time) and sunrise was at about 6:03 (Pacific Daylight Time).

Although the flight data summary reports that the sun was several degrees above the horizon at 5:55 a.m. this must still have been before sunrise to a ground observer. Despite the possibility that some of it may have been obtained after sunrise, there is little or no evidence of this in the infrared imagery and any effects due to solar heating must be minor. The July 29 imagery is generally satisfactory for geologic interpretation and because it and that taken during the daytime on July 28 are superior to the other infrared surveys, this report is concerned solely with the results shown by the imagery of July 28 and 29. Although these data were collected more than a month after the main earthquake on June 27, earthquake activity and fault movement were continuing. Eaton (in Brown and others, 1967, p. 60) reports an aftershock rate, recorded at the Gold Hill station about midway between Parkfield and Cholame, of 19 quakes per day for July 28, and Wallace and Roth (in Brown and others, 1967) have shown that detectable fault movements continued into August.

Interpretation of imagery

General discussion.--Much of the information contained in the selected samples of early morning (figures 2A, 3A, 4A, and 5A) and midday (figures 2B, 3B, 4B, and 5B) infrared imagery can be easily related to terrain and cultural features shown on conventional aerial photographs (figures 2C, 3C, 4C, and 5C). The illustrations of infrared imagery in this report have been enlarged from the original film strip.

Although the infrared radiation depicted in the imagery is a function of both absolute temperature and emissivity, the variations in emissivity are probably relatively minor, and most of the contrast

shown in the imagery is presumed to be a function of temperature. As reproduced here the infrared imagery shows warm areas in light tones and cold areas in dark tones. Thus in figures 2A and 2B, for example, surfaced roads, slightly cooler than their surroundings in the daytime imagery (figure 2B), are distinctly warmer than the adjoining areas in the early morning imagery (figure 2A). Similarly, in the same set of imagery, the bed of Cholame Creek is relatively cold in the daytime imagery and is evident as a dark, well-defined drainage system in a background of relatively warm grass-covered terrain. The creek bed is much less evident in the early morning imagery of figure 2A, but can be distinguished as slightly cooler than its surroundings (right of center of figure 2A) or slightly warmer than its surroundings (left of center of figure 2A). The cause of the apparent differences in early morning infrared radiation from the creek bed is not known but it could be a result of: 1) standing or running water in the lower part of the stream (right side of figure 2A) and a dry creek bed upstream, 2) warmer run-off from irrigated fields near the left margin of figure 2A as opposed to normal or near normal groundwater temperatures downstream, or 3) response of the imaging system to changing infrared temperatures in the terrain on either side of the stream bed (in this case, the stream bed infrared temperature may be essentially the same throughout figure 2A, but because of system response to the entire field of scan it appears relatively cool in one area and relatively warm in another).

Some features are clearly visible on both daytime and early morning imagery. Examples are the surfaced roads and stream beds mentioned above, irrigated fields which are generally cooler than their

surroundings, ponded water or that in tanks--relatively cool in the daytime imagery but distinctly warmer than nearby areas at sunrise--, and some cultivated fields which vary in their infrared signatures but which commonly exhibit a contrast with natural vegetation.

Other features are readily identifiable only on one set of imagery or the other. A fence near the center of figure 2B is clearly evident under daytime conditions but is only locally apparent in figure 2A. A cultivated field northeast of the Jack Ranch headquarters is clearly cooler than nearby natural vegetation in the early morning imagery (figure 3A) but is barely distinguishable in figure 3B. A power line (left of center of figure 3B) can be identified by the thermal contrast of its steel towers and by a cool band associated with a road that follows it, but it is evident in figure 3A (early morning) only by a warmer-than-normal line that marks the power line road. An airstrip which shows as a warm band in the early morning imagery of figure 3A cannot be identified in the daytime imagery of figure 3B.

Geologic interpretation.--Numerous examples of relations like those described above are evident on the infrared imagery illustrated, but even a cursory examination of the imagery shows that most of the information conveyed in it concerns differences in vegetation type and stages of growth. It is therefore difficult to interpret geologic relations directly from the infrared imagery. But geologic information can be extracted from some of the vegetation patterns where these are controlled by geologic conditions. Interpretation of this sort is analogous to that used in the geologic interpretation of conventional aerial photos, where certain vegetation types are known to grow

selectively on some rock units and not on others, or where fault zones or permeable strata provide near-surface groundwater that favors growth.

The amount of geologic data that can be extracted from vegetation patterns varies greatly with climate, rock type, structural complexity, and soil depths as well as with other variables. In general, the level of interpretation possible is considerably less than where bedrock units are exposed at the surface, and soil and vegetative cover is minimal. Yet, because much of the earth's surface is covered with plant growth, geologic interpretation of vegetative patterns has widespread applicability, and used together with other terrain analysis techniques it is often the only means of quickly obtaining geologic data by remote means.

Although the imagery shown here was obtained for a study of the San Andreas fault, it contains additional geologic information as well. Alluvial deposits of Cholame Valley and its tributary valleys are well defined, and are manifested in the early morning imagery as darker or cooler areas surrounded by the warmer tones of hilly areas covered with natural vegetation. This contrast is most evident where the alluvium has been cultivated and supports crops, but it is also apparent in natural vegetation. It is particularly clear in the left 1/3 of figure 3A where old meander scars of Cholame Creek impinge against the hilly bedrock terrain to the northeast. To a lesser extent, the alluvium-bedrock contact can also be detected in the daytime imagery (see especially figure 2B). Although several factors may contribute to the characteristic infrared pattern of the alluvium it seems to be chiefly due to the density and vitality of vegetation there, a result in turn of richer soil and relatively abundant soil moisture in the alluviated areas. For much of the area shown in figures 2 through 5,

alluvial deposits can be more easily and more accurately delineated on early morning infrared imagery than on conventional air photos or by other known techniques. Interpretations of this sort, however, must be made cautiously, for under certain conditions cool thermal signatures for valley areas are produced by cold air that accumulates at low elevations during the night (E. Wolfe and M. Clark, personal commun., 7-1-68).

Another contrast of possible geologic significance is that shown by hilly areas on opposite sides of the San Andreas fault. The hills southwest of the fault, in the bottom half of figures 2 and 5 and in the bottom 1/3 of figures 3 and 4, are intricately dissected and are covered with both oak and native grasses. Those northeast of the fault, in the upper part of figures 2 through 5 are less dissected and are chiefly grass covered. These differences are shown in both daytime and early morning imagery: tree cover is most evident in the daytime imagery but the subtle tonal contrast is more obvious in the early morning imagery where the upland areas northeast of the fault appear distinctly warmer and brighter than those to the southwest. Degree of dissection can be observed about equally well on either set of imagery.

Nongeologic controls may be responsible for some or all of the contrast, but published geologic maps (Jennings, 1958; Marsh, 1960; Dickinson, 1963, 1966a,b) show that the near surface rocks of the two upland areas differ markedly in their physical and chemical properties (figure 6). Southwest of the fault the Cholame Hills, shown in the lower parts of figures 2 through 5, are underlain in most places by the Paso Robles formation of late Tertiary to Quaternary age, a sedimentary

unit of nonmarine origin, composed chiefly of sand, silt, clay, and gravel. Across the fault to the northeast the hill areas, shown in the upper part of figures 2 through 5, are underlain by complexly folded and faulted marine sedimentary rocks of Mesozoic and Tertiary age, and by a tectonic complex of cataclastically deformed Mesozoic sedimentary rocks that have been invaded by serpentinite. Although it is difficult to prove such a relationship, it seems likely that these geologic differences, through their effect on native vegetation, are responsible for some of the contrast seen in the imagery.

Probably the most striking infrared anomaly shown in the pre-sunrise imagery is that associated with Gold HIll, which shows in figures 3A and 4A as a bright warm area. This anomaly coincides very closely with a lens-like mass of hybridized metamorphic and igneous rocks (figure 6) described by Hay (1963) as amphibolite and metamorphosed crystalline rocks that superficially resemble a medium grained diorite.

Gold Hill is surrounded by relatively young terrace deposits and alluvium but similar crystalline rocks crop out in a small area about 0.6 mile northeast of the crest of Gold Hill. This relatively small exposure of Gold Hill lithology is identifiable in figure 3A as bright warm area similar to the anomaly associated with the larger mass of crystalline rock.

Without evidence to the contrary, one might account for the Gold Hill anomaly by its slope orientation. The thermal anomaly is associated with a west-facing slope that presumably must attain its maximum temperature later in the day than adjoining nearly-horizontal lowland areas. Accordingly the nocturnal cooling curve for the west slope of Gold Hill could lag behind similar curves for lowland terrain, and

an early morning thermal anomaly would be produced over the west slope; such an anomaly would be largely independent of geologic conditions. Two lines of reasoning argue against this explanation. First, the small warm area northeast of Gold Hill--and also underlain by crystalline rocks--is in terrain with low relief, yet it exhibits a warm infrared signature resembling that of Gold Hill. Second, hill slopes similar in height, gradient, and orientation to the west slope of Gold Hill are found elsewhere along the northeastern side of Cholame Valley (notably near the upper left margin of figure 2A), yet none of these show evidence of higher-than-normal radiation. I therefore conclude that hill slopes shown in the early morning imagery have attained a state of thermal equilibrium and that the Gold Hill anomaly has some other cause--most likely a geologic influence because of the small anomaly associated with similar rock types to the northeast.

The crystalline rocks of Gold Hill are well exposed in only a few places and most of the area underlain by these rocks is mantled with a thin soil that supports a sparse native grass cover on the southwest slope and a grass and oak cover on the northeast slope. The thermal infrared characteristics of Gold Hill are therefore probably not a direct result solely of bedrock lithology, but are due to a combination of geologically-controlled surface or near-surface conditions. The relative sparseness of grass cover, the thin soil, and the presence of dense crystalline rock at shallow depth probably combine to produce a surface that, during the nocturnal cooling cycle, emits more radiant energy than its surroundings. Evidence to support these conclusions is based chiefly on observations at a test site where thermal conditions in

barren soil, grass covered soil, and living vegetation were obtained during the hours between 8 p.m. and 8 a.m.--the results of these observations are discussed elsewhere in the report. Other infrared anomalies, similar in tone and contrast to those at Gold Hill and to the northeast, are apparent at a number of places on the imagery; few of these, if any, appear to be lithologically controlled and they apparently are due to other, unknown causes.

Anomalies along the active trace of the San Andreas fault.--The infrared imagery of figures 2 through 5 show a variety of terrain features and vegetation contrasts that are alined along the active traces of the San Andreas fault. None of these appear to be due solely to the 1966 episode of fault movement, nor was any evidence found of infrared anomalies caused by heat conducted from the earth's interior or by geothermally heated groundwater.

Many of the terrain features along the fault, such as offset streams, straight, fault-controlled stream segments, scarps, and sag depressions are better seen and more readily interpreted from conventional black and white panchromatic aerial photos than from the imagery. For this reason, no further evaluation of the terrain features is attempted in this report.

Some of the vegetation patterns found along the fault are more clearly defined in the infrared imagery than in other available remote sensing systems. Some of these are, as far as is known, shown only by the infrared imagery. The following discussion concerns a representative sample of the infrared anomalies that appear along the fault zone and that seem to be caused by vegetation patterns related to fault trace

geologic conditions. Nearly all of these examples are best expressed on the early morning imagery of figures 2A, 3A, 4A, and 5A.

A barely perceptible infrared contrast is shown along the fault trace in the left center part of figure 2A immediately southwest of the Parkfield road. A dark cool area northeast of the fault contrasts with a very slightly warmer area across the fault to the southwest. Field inspection of this area disclosed no visible soil differences nor was evidence found for near surface groundwater on either side of the fault, but the fault trace marks the approximate boundary between a relatively thick stand of dry grass (apparently dead on July 28, 1968--exactly 2 years after the imagery was obtained) northeast of the fault, and similar but sparser dry grass southwest of the fault. The anomaly thus appears to be due to a vegetation difference controlled by the fault, but its precise cause is unknown. Because the fault commonly serves as a barrier to groundwater the vegetation contrast may be a result of different groundwater levels across the fault; or, because some wells in Cholame Valley have encountered salt water and others have yielded fresh water, a soil salinity contrast may be the cause. Whatever the cause, the fault trace appears to be of prime influence in controlling its effect on vegetation.

A well-defined cool infrared anomaly about 0.4 mile north of the Jack Ranch headquarters is apparent on both figures 3A and 3B. It appears on figure 3B as a narrow arcuate band, gently concave towards the west. This pattern coincides with green, living vegetation growing at the base of a low scarp bordering a sag depression along the most recent trace of the fault. Spring lines along the fault here coincide

with the vegetation pattern and account for its localization in a terrain that is elsewhere covered with dry grass. A much smaller but similar anomaly is visible on the daytime imagery (figure 3B) about 0.7 mile north of Jack Ranch headquarters, it appears as a darker cool spot and is produced by a small plot of green leafy vegetation growing in the center of a sag depression that is otherwise marked by bare soil (fine sandy silt with scattered coarse sand grains). This relatively small feature is not apparent on the early morning imagery, and it is of interest chiefly because it provided a convenient site at which to compare thermal and infrared characteristics of different surface environments.

A well marked lineament along the San Andreas fault near the center of figure 5A extends for about a mile northwest of Parkfield where it appears as a light-toned warm strip cutting through surroundings with more variable infrared characteristics. This lineament can also be identified in the daytime imagery of figure 5B but it is less distinct there than in the early morning imagery. It can be related to untilled sparsely wooded grassland along a narrow trench that is controlled by a trench that contains the trace of most recent faulting. The relatively sparse dry grassland of the trench area seems to radiate (or reflect) more infrared energy than adjoining tilled areas, which support a denser grass cover.

Surface observations

Purpose and scope.--To help evaluate the aerial infrared imagery a small area on the ground was selected where ground based radiometer and temperature measurements could be obtained under conditions similar to

those encountered during the overflights. Ground measurements were scheduled for a 24-hour period between July 25 and July 30, 1968 so that sun positions and solar heating effects would approximate those during the flight. A reasonably close approximation to flight time conditions was achieved by reference to the pilot's flight log of weather conditions on July 28-29, 1966 and to U.S. Weather Bureau records for weather at Paso Robles and Priest Valley, the closest comparable stations for which data were available (see table I).

Because most of the characteristic infrared patterns observed in the airborne imagery seemed to indicate differences in vegetation patterns, the test area was selected to obtain temperature data on dry barren soil, on dry grass, and on a plot of green, living vegetation. Only a small area and a few vegetation types could be examined because the infrared radiometer used is dependent on an external power source, in this case an automobile battery, and it is generally impractical to move the power source once a series of measurements have been started.

The influence of near surface air temperature gradients, which can materially affect infrared imagery, was also considered important. For this reason it was desirable to select a low area where air temperatures at several heights above the ground could be compared as a means of determining whether cold air accumulated at low elevations.

For obvious reasons the temperature and other data obtained from the test area cannot be rigorously applied to the airborne imagery. It is useful, however, in showing the general range of some of the parameters depicted in the imagery and in suggesting reasons for some of the imagery contrasts.

Table I

Comparison of U.S. Weather Bureau air temperatures in °Centigrade for July 28-29, 1966 and July 29-30, 1968

	7-28-66 (7-29-68)		7-29-66 (7-30-68)	
	Low	High	Low	High
Paso Robles	11 (17)	37 (36.8)	6.7 (13.4)	35 (35.5)
Priest Valley	7.8 (11.6)	33 (35.5)	8.9 (15.5)	35 (33.5)
Average difference 7-68	4.9	+1.2	+6.6	-0.7

Test area and instrumentation.--The test area selected is a small sag depression about 0.68 mile southwest of the summit of Gold Hill and about 0.7 mile northwest of the Jack Ranch headquarters. It lies along the 1966 fracture zone of the San Andreas fault and is about midway between stations F15 and F16 of the map of the fault break (Brown and Vedder, 1967, fig. 2, p. 7). It is underlain by alluvium, but is about 20 feet above the present level of Cholame Creek. A sketch planimetric map of the test area (figure 7) shows its shape and the location of instrument sites from which data were obtained. Relief in the vicinity of the test area is low; the floor of the sag depression is level and is surrounded by terrain from about 3 to 20 feet higher, with greatest relief northwest of the depression.

Three types of temperature measuring devices were used. Thermometers were placed at variable heights on stakes at S-1 and S-2 (figure 7) to record near surface air temperature gradients. At S-1, 3 thermometers were located with their bulbs 7 inches, 21 inches, and 34 inches above the ground surface. A single thermometer was located about 30 inches above the ground at S-2, or about 65 inches higher than the bare earth surface of the sag. All thermometers were exposed to direct radiation. Recording thermographs were located at T-1, T-2, and T-3 (figure 7) with their sensing elements buried beneath 2 inches of soil; after burial, the surface at each of these points was restored as nearly as possible to its undisturbed state. Infrared temperatures were obtained on green vegetation near T-1, on bare earth near T-2, and on dry grass near T-3.

Thermometers used were mercury-type with a range from -10 to 110°C and graduated at 1° intervals. They were previously calibrated and found to be accurate to within 1°C for the range of temperature values recorded.

Two types of thermographs were used. Those at T-2 and T-3 were Electric Autolite model 1000 and recorded in the range from 20 to 220°F. The thermograph at T-1, also an Electric Autolite model 1000, had a temperature range of 20 to 120°F. Calibration of the thermographs against a mercury thermometer standard indicated they agreed to within 2°F for the range of temperatures recorded. Selected thermograph temperature values were later converted to centigrade for comparison with other readings.

Infrared temperatures were obtained with a Barnes Engineering Company IT-3 radiometer (8 to 14 μ spectral range) with a scale calibrated from -10 to 45°C. Calibration against a water standard and a mercury thermometer showed the measured infrared temperature to vary no more than 0.8°C from the standard in the range from 4 to 45°; for most of the range measured in the field, variation from the standard was less than 0.5°C. Because of the 45°C upper limit of the radiometer, infrared temperatures were obtained only during the hours from 2000 to 0800 P.D.T. The lack of infrared temperature during daylight hours is not critical because nearly all of the anomalies shown on the imagery are most emphasized in the pre-sunrise flight.

Besides the temperature records, relative humidity was determined for air in the vicinity of the green vegetation at T-1 and for air about 3 feet above the dry grass covered terrain. These measurements were made with a hand aspirated psychrometer, chiefly to facilitate humidity

determinations within the leafy growth of green vegetation. This instrument was not previously calibrated, but the dry bulb readings generally agreed to within 1°C of the temperature values obtained at S-1 and S-2. One or two of the relative humidity determinations (figure 10) may be erroneous for they plot off the general trend shown by the others.

Nonrecording instruments (thermometers, radiometer, and psychrometer) were generally read at hourly intervals from 0930 to 1530 hours (P.D.T.) July 29, 1968 and from 2000 hours July 29, 1968 to 0800 hours July 30, 1968. Humidity determinations in vegetation were made at 2 hour intervals. The continuously recording thermographs were operating throughout the observation period, but only hourly data are summarized here.

Discussion of data.--Data obtained at the test area are summarized in figures 8, 9, and 10.

Figure 8 summarizes thermograph records of soil temperature, normal air temperature, and local weather conditions that affect some or all of the temperature measurements. None of these data are directly related to the infrared imagery, which measures only surface temperatures. They are of interest, however, because they document the effects of solar heating and nocturnal cooling and because they show that heat losses from the surface are at a nearly constant, low rate during the early morning hours.

Also of interest is the apparent insulating effect shown by dry grass cover in the thermograph record from T-3. Although during the period of maximum solar heating the grass-covered soil is warmed at about the same rate as bare soil and attains about the same maximum

temperature, it cools more slowly and its minimum temperature is several degrees warmer than the bare soil. This suggests that early morning heat loss from dry grass covered areas may be somewhat lower than that from bare soil. This suggestion is apparently confirmed by the infrared temperature curves of figure 9 which show generally higher radiation temperatures for the bare surface of the sag depression during the early morning hours. It does not agree however with some of the relations shown in the imagery, for many bare soil areas shown there are colder than grassy terrain.

Soil temperature beneath green vegetation (curve T-1 of figure 8) shows a maximum at about 1300 hours that is well below the other soil temperature curves and is even less than normal air temperature--an effect due partly to shading by the leafy plant cover and partly to transpiration (see relative humidity curves of figure 10). The early morning minimum for soil temperature beneath the vegetation is the same as for bare soil, but this might not be so if the vegetation-covered area were larger. The small plot of leafy plant growth is apparently the only feature within the test area that can be resolved in the infrared imagery and it is identifiable only in the daytime imagery as a cool dark spot.

The infrared temperatures of figure 9 are more directly related to contrasts shown in the imagery, provided flight-time conditions were closely approximated during the recording period. The infrared temperature curves show the green vegetation of the sag depression to be the coolest of the 3 surface types measured. Although test area vegetation was not detected in the early morning imagery, larger masses of similar

vegetation in nearby sags were, and they consistantly show markedly cooler than their surroundings. Larger living plants--oak trees for example--do not show on the early morning imagery; presumably their temperature contrast with their surroundings is less than that of the smaller plants.

The discrepancy between imagery and observational data for dry grass and bare ground, mentioned previously, possibly may be explained by the relations shown in figure 9 and by minor differences in air temperature at the time of flight and the time data were obtained at the test area. Table 1 compares the high and low temperatures at Priest Valley and Paso Robles for these two periods and shows that although daytime maxima are similar, the early morning minimum was several degrees colder the morning the imagery was obtained than it was when test area data were gathered. Figure 9 and the thermograph records of figure 8 suggest that bare soil cools more rapidly than grass covered areas. The radiometer measurements (figure 9) for bare soil show a slightly steeper average slope and a sharper early morning minimum than do comparable measurements for dry grass. With early morning temperatures several degrees cooler than those measured, it seems possible that infrared temperatures of bare soil could drop below those for grassy areas. Although this seems a likely explanation for some of the anomalous relations shown by the imagery other explanations are also possible.

The radiometer records of two of the measured surfaces (dry grass and bare soil) show a marked increase before 0600 even though no direct light from the sun was visible until about 0615. This temperature rise is not seen in the normal air temperature record nor was it measurable

on green vegetation (figure 9). Because a lightening of the sky (dawn) began about 0500, the pre-sunrise infrared temperature rise is possibly caused by reflected infrared radiation from the sky. Alternatively, it may be due to a scattered cloud cover which began to form in the east and was broken overhead at 0600. Sky infrared temperature at 0600 was -2° centigrade; during clear periods the sky infrared temperature was much colder than -10° centigrade, the lower hand limit of the radiometer. Of these possibilities the latter seems the most likely, for other observers (M. Clark and E. Wolfe, personal commun., 8-1-68) have recorded stable pre-sunrise infrared temperatures under clear sky conditions.

Conclusions

Examination of the infrared imagery of July 28-29, 1966 coupled with ground measurements made two years later yields the following conclusions:

1. The infrared imagery shows no direct evidence of the 1966 Parkfield-Cholame fault movement nor does it show evidence of indirect effects caused by such phenomena as disturbed ground water levels or geothermally heated waters.

2. It does afford indirect evidence, in the form of vegetation patterns, that permit local identification of the San Andreas fault. Such evidence is inadequate to trace the fault continuously through the imaged areas and in general the fault is delineated better on panchromatic aerial photos. In a few places, however, the infrared imagery is superior to panchromatic photography for this purpose.

3. Some geologic units can be better identified and more accurately delineated on the infrared imagery than by other remote sensor systems. In the imagery evaluated here, alluvium, crystalline rocks, and possibly late Tertiary and Quaternary nonmarine strata are identifiable and

crudely mappable by their infrared patterns. The degree of precision in delineating such units, while superior to other remote systems, falls far short of that attainable by on-the-ground field investigation; moreover, field investigation discloses many other geologic units that are not resolved by the infrared imagery.

4. Most of the characteristic patterns that distinguish different rock units in the infrared imagery are due to vegetation contrasts which are probably related to the physical and chemical properties of the soil and to its moisture content. Insofar as these properties reflect underlying bedrock character, the vegetation patterns can be successfully used for geologic interpretation. Such patterns are best seen on early morning imagery.

5. Because many variables can affect the infrared imagery, geologic interpretation must be cautious. Microclimate effects, cloud cover, wind, surface geology, vegetation type, ground conditions, and changes in the elevation of the groundwater table are only a few of the influences that can completely alter the infrared regime of areas that are otherwise identical. It is nearly impossible to evaluate all these variables thoroughly during flight coverage of an area of the size reported on here, and it is equally difficult to duplicate flight conditions for a long enough period to perform the evaluation later. However, clues to some of these effects are generally present in the imagery and others can be evaluated at a sample level by ground observations. Although a rigorous geologic evaluation of imagery of so large an area is impractical and would probably be unrealistic, a general appraisal can be useful if attention is given to the non-geologic effects.

6. The resolution of ground detail and the obvious sensitivity of the imaging system encourages further experimentation over areas of active faulting especially to identify possible secondary effects of faulting in areas where groundwater levels are known to be near the surface. Ideally, such future experiments should involve ground temperature and other observations during the flight period but this is not a vital requirement.

References cited

Brown, R. D., Jr., 1966, Geologic evaluation of radar imagery: San Andreas fault zone from Stevens Creek, Santa Clara County to Mussel Rock, San Mateo County, California: NASA Technical Letter 45, 6 p.

Brown, R. D., Jr., Vedder, J. G., Wallace, R. E., Roth, E. F., Yerkes, R. F., Castle, R. O., Waananen, A. O., Page, R. W., and Eaton, J. E., 1967, The Parkfield-Cholame earthquakes of June-August 1966--surface geologic effects, water resources aspects, and preliminary seismic data: U.S. Geol. Survey Prof. Paper 579, 66 p.

Brune, J. N., and Roy, R. F., 1968, Heat flow and stress along the San Andreas fault near Hollister, California [abs.]: Program of the 64th Annual Meeting, Geological Society of America, Tucson, Arizona, April 11-13, 1968, p. 42.

Dickinson, W. R., 1963, Tertiary stratigraphic sequence of the Hancock Ranch area, Monterey and King Counties, California, in Guidebook, to the geology of the Salinas Valley and the San Andreas fault: Am. Assoc. Petroleum Geologists-Soc. Econ. Paleontologists and Mineralogists, Pacific Sec., Ann. Spring Field Trip 1963, p. 47-53.

_____ 1966a, Table Mountain serpentine intrusion in California Coast Ranges: Geol. Soc. America Bull., v. 77, no. 5, p. 451-472.

_____ 1966b, Structural relationships of San Andreas fault system, Cholame Valley and Castle Mountain Range, California: Geol. Soc. America Bull., v. 77, no. 7, p. 707-726.

Fischer, W. A., Moxham, R. M., Polcyn, F., and Landis, G. H., 1964, Infrared surveys of Hawaiian volcanoes: Science, v. 146, p. 733-742

Hay, E. A., 1963, Age and relationships of the Gold Hill pluton, Cholame Valley, California, in Guidebook to the geology of the Salinas Valley and the San Andreas fault: Am. Assoc. Petroleum Geologists-Soc. Econ. Paleontologists and Mineralogists, Pacific Sec., Ann. Spring Field Trip 1963, p. 113-115.

Jennings, C. W., 1958, Geologic map of California, Olaf P. Jenkins edition, San Luis Obispo sheet: Calif. Div. Mines, scale 1:250,000.

Marsh, O. T., 1960, Geology of the Orchard Peak area, California: Calif. Div. Mines Spec. Rept. 62, 42 p.

Wallace, R. E., and Moxham, R. M., 1967, Use of infrared imagery in study of the San Andreas fault system, California, in Geological Survey Research 1967: U.S. Geol. Survey Prof. Paper 575-D, p. D147-D156.

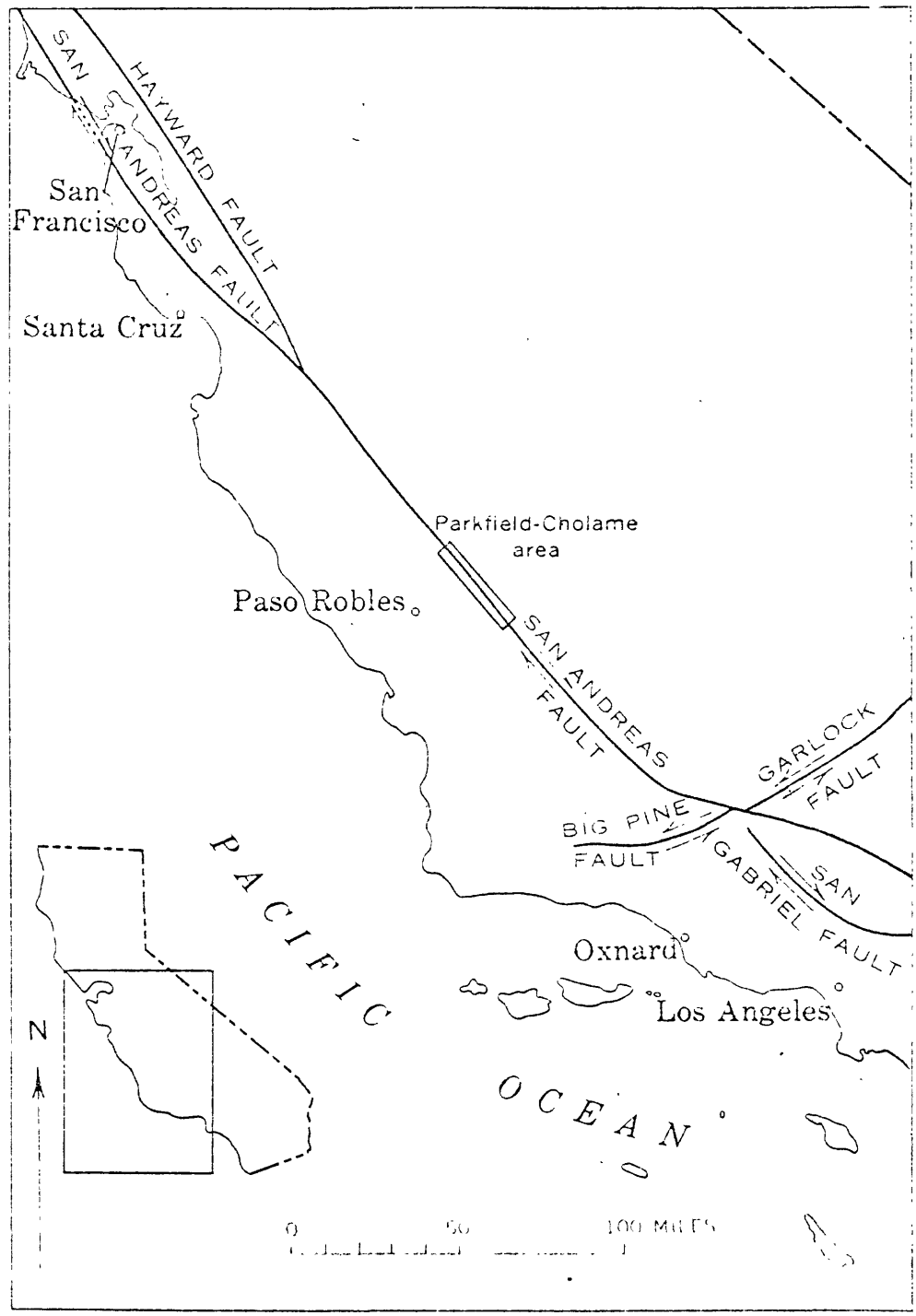

Figure 1.--Part of the San Andreas fault zone and the location of the Parkfield-Cholame area.

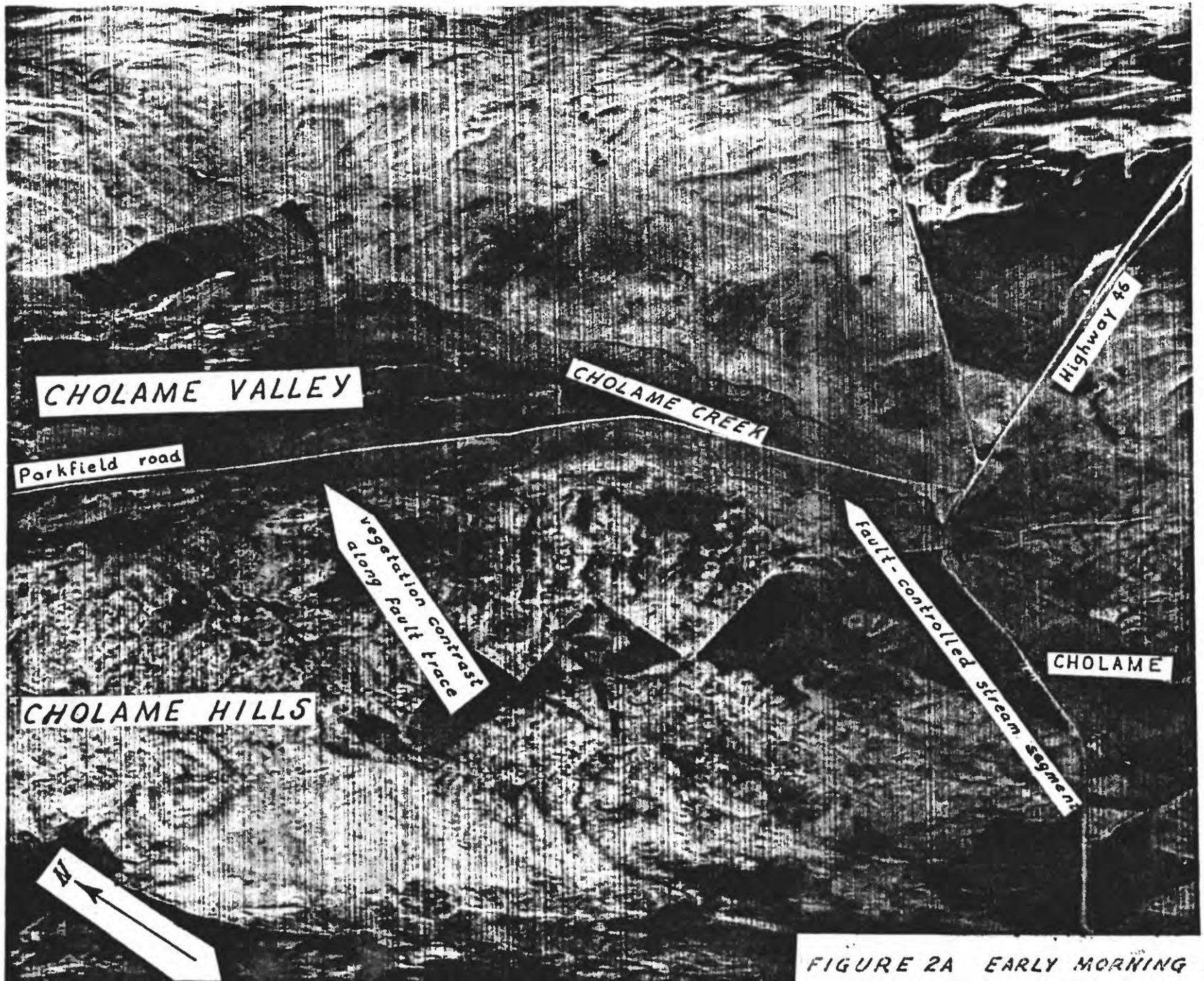

FIGURE 2A EARLY MORNING

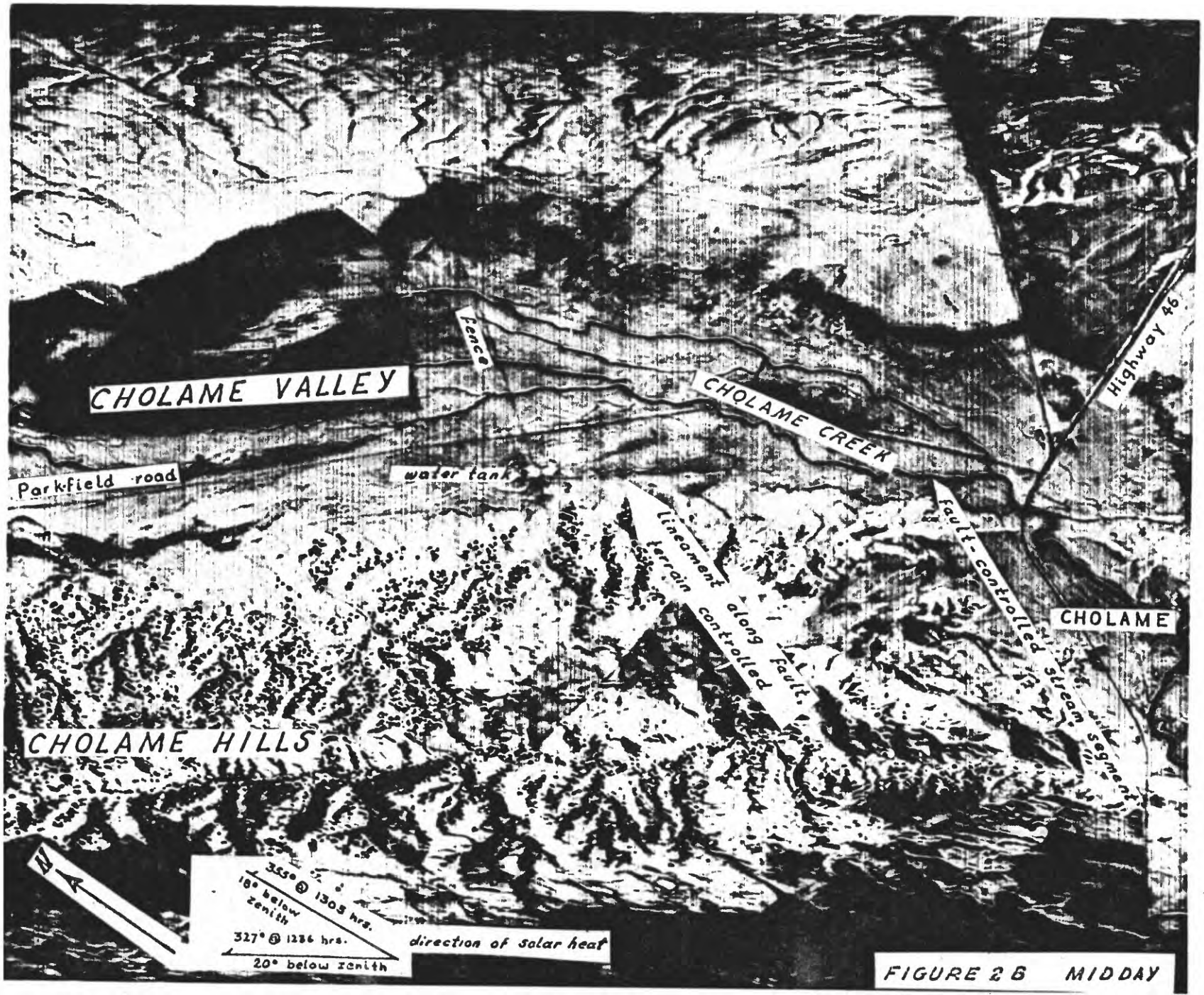

FIGURE 26 MIDDAY

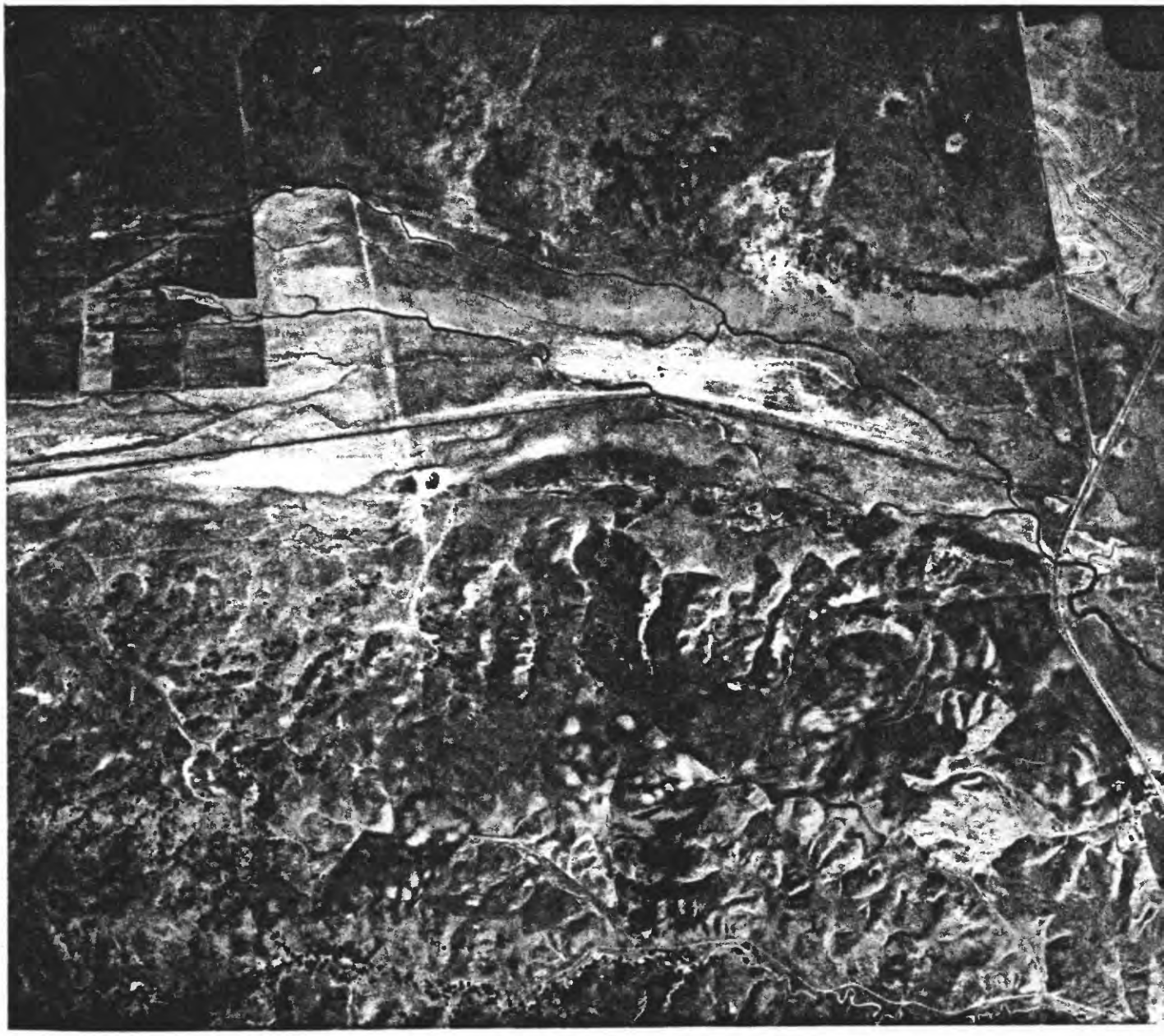

FIGURE 2C PANCHROMATIC

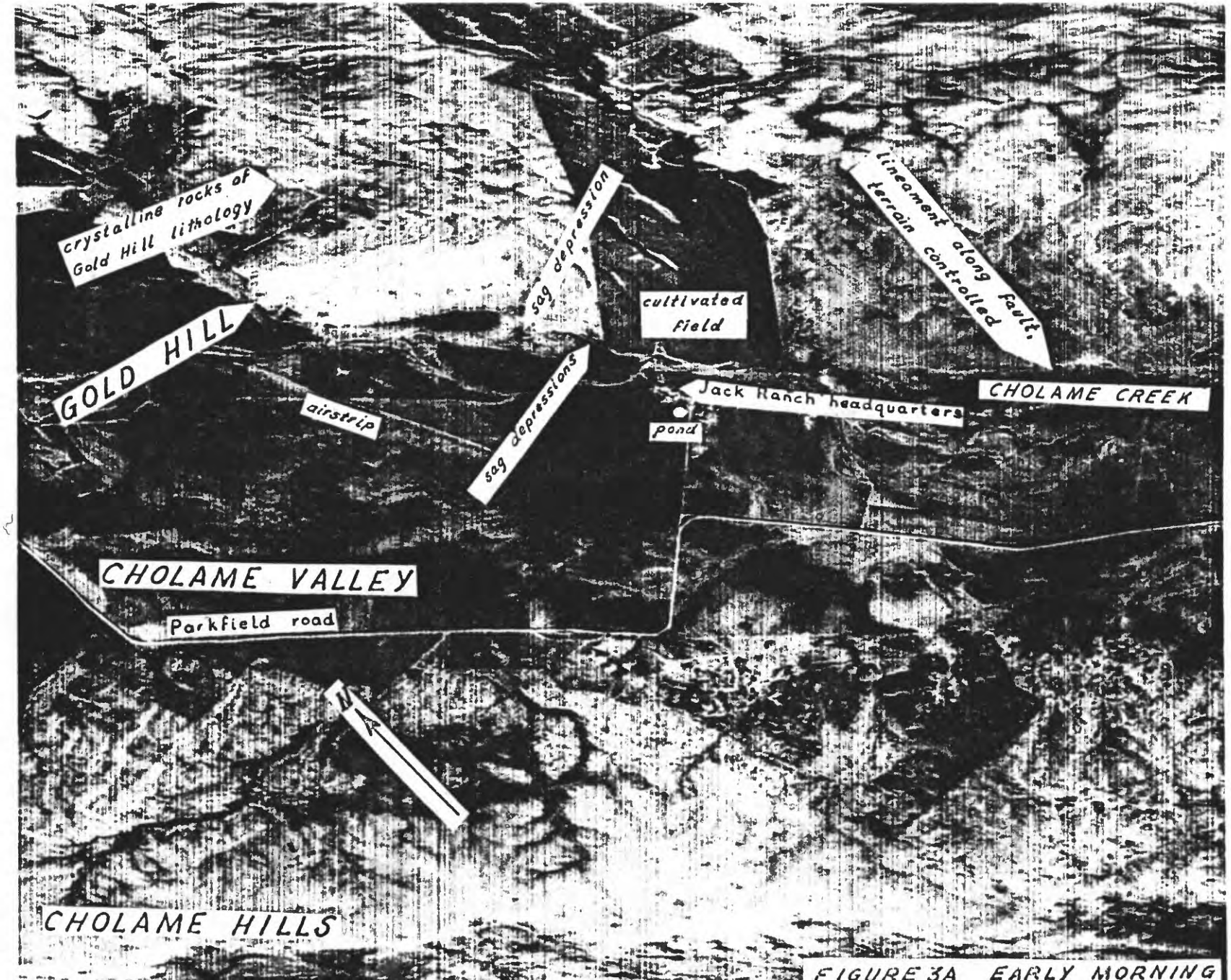

FIGURE 3A. EARLY MORNING

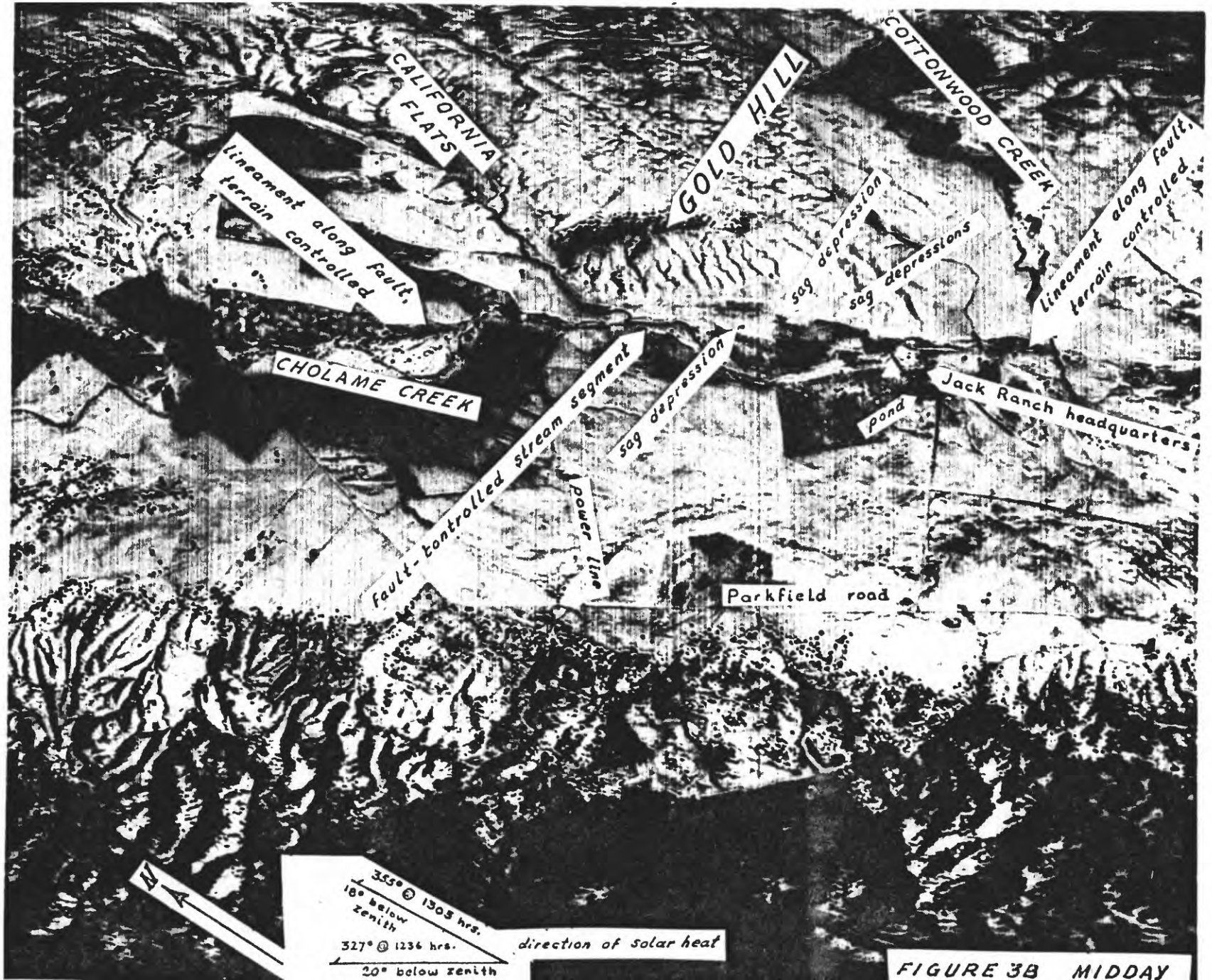

FIGURE 3B MIDDAY

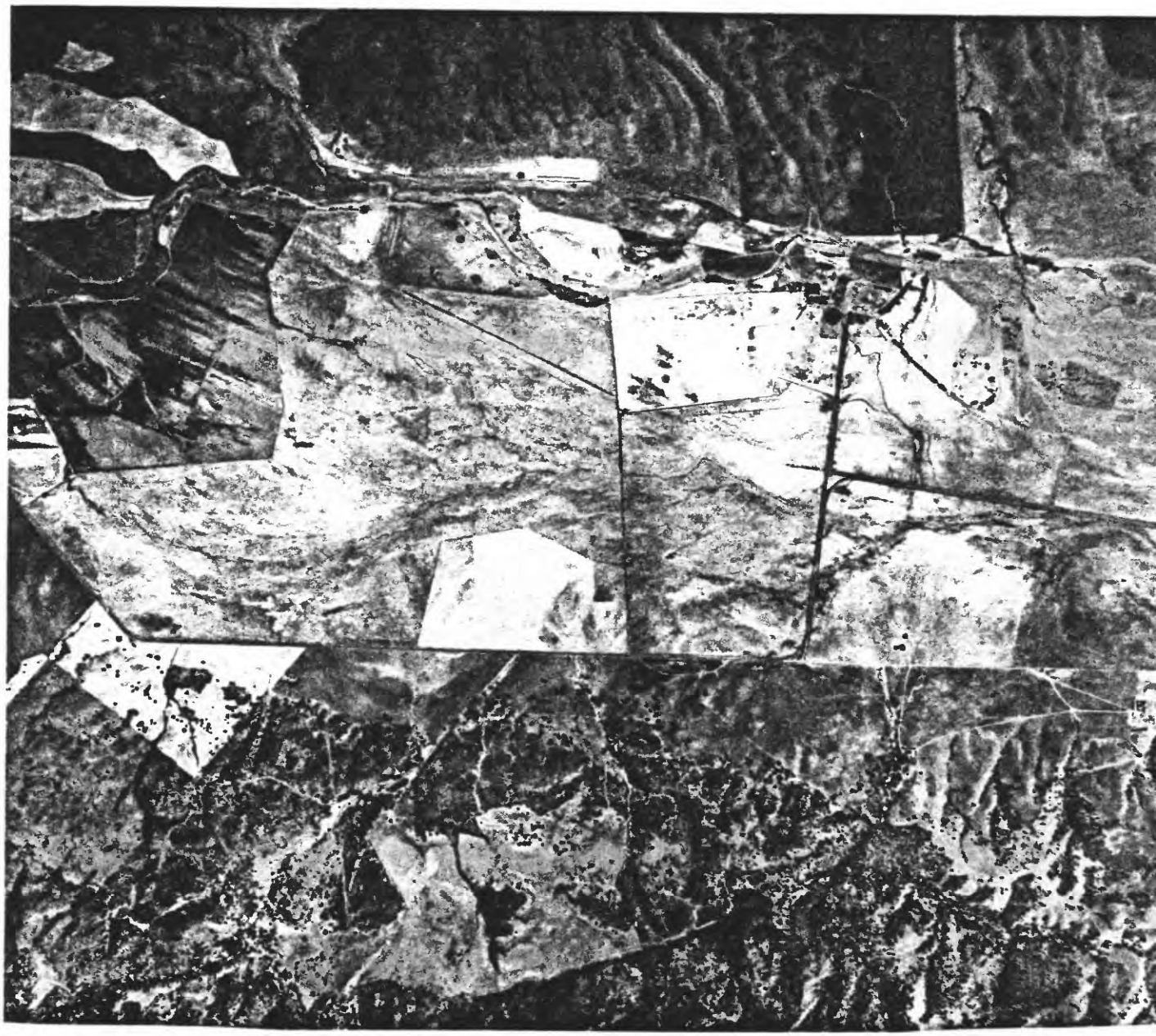

FIGURE 3C PANCHROMATIC

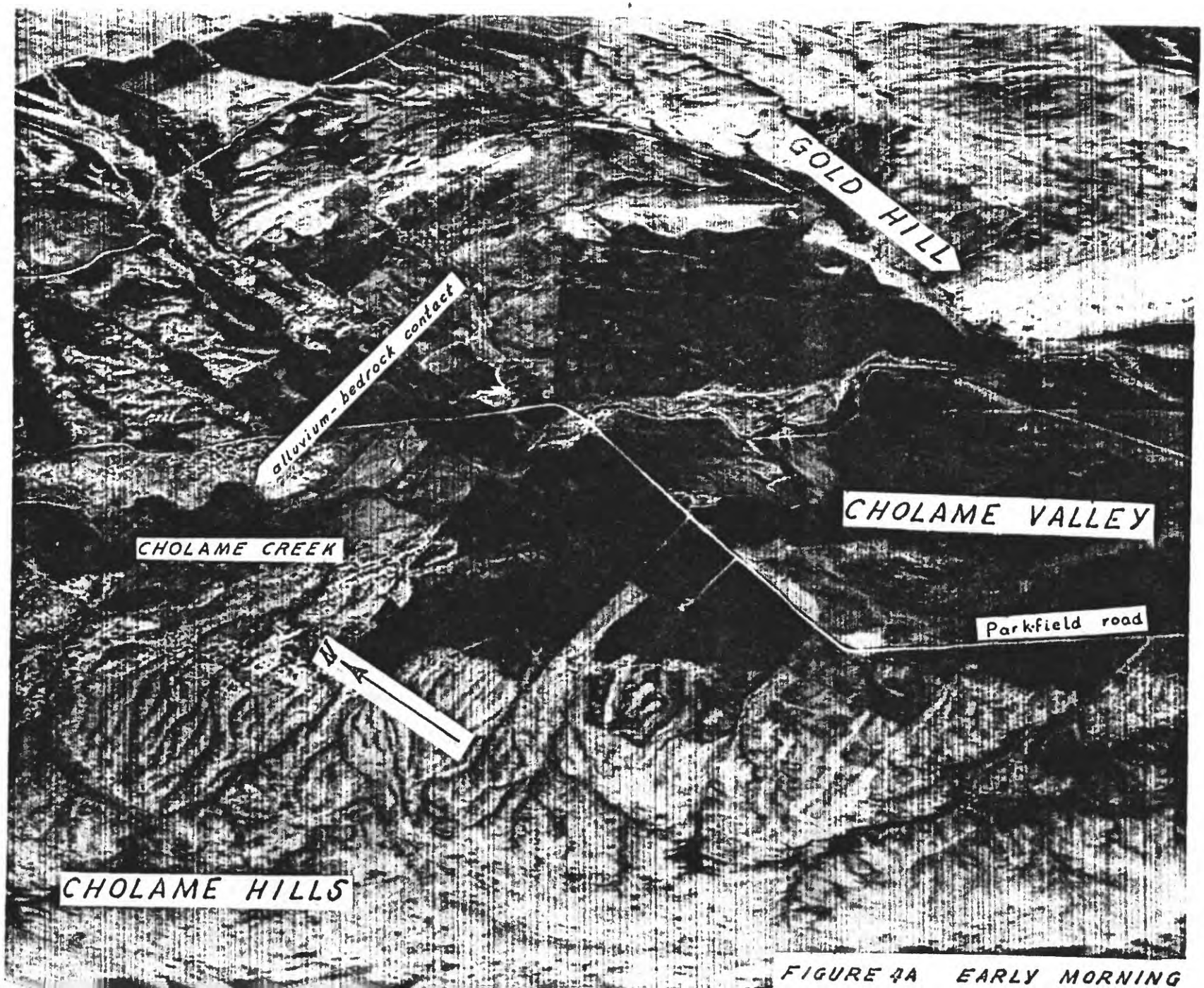

FIGURE 4A EARLY MORNING

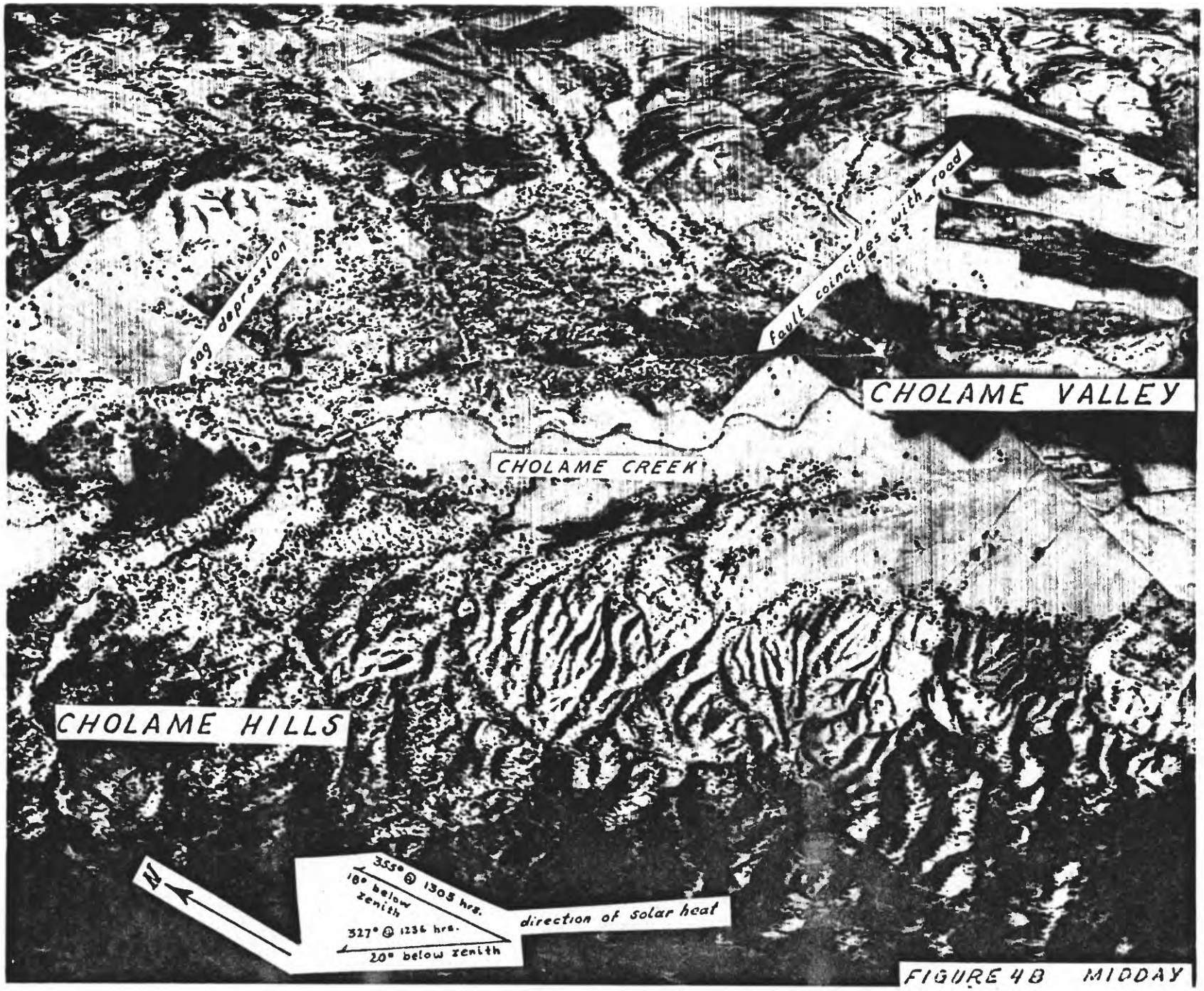

FIGURE 48 MIDDAY

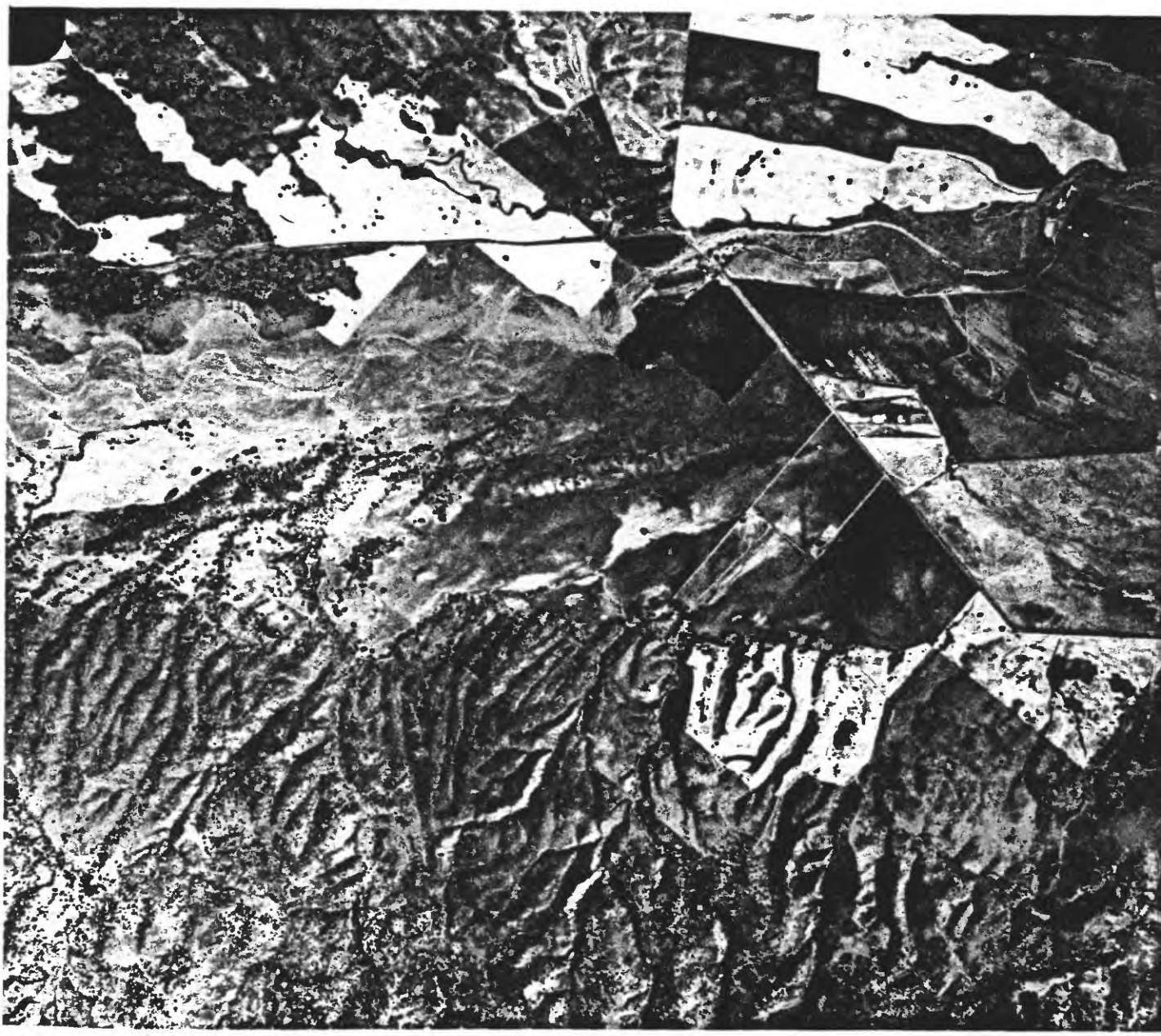

FIGURE 4C PANCHROMATIC

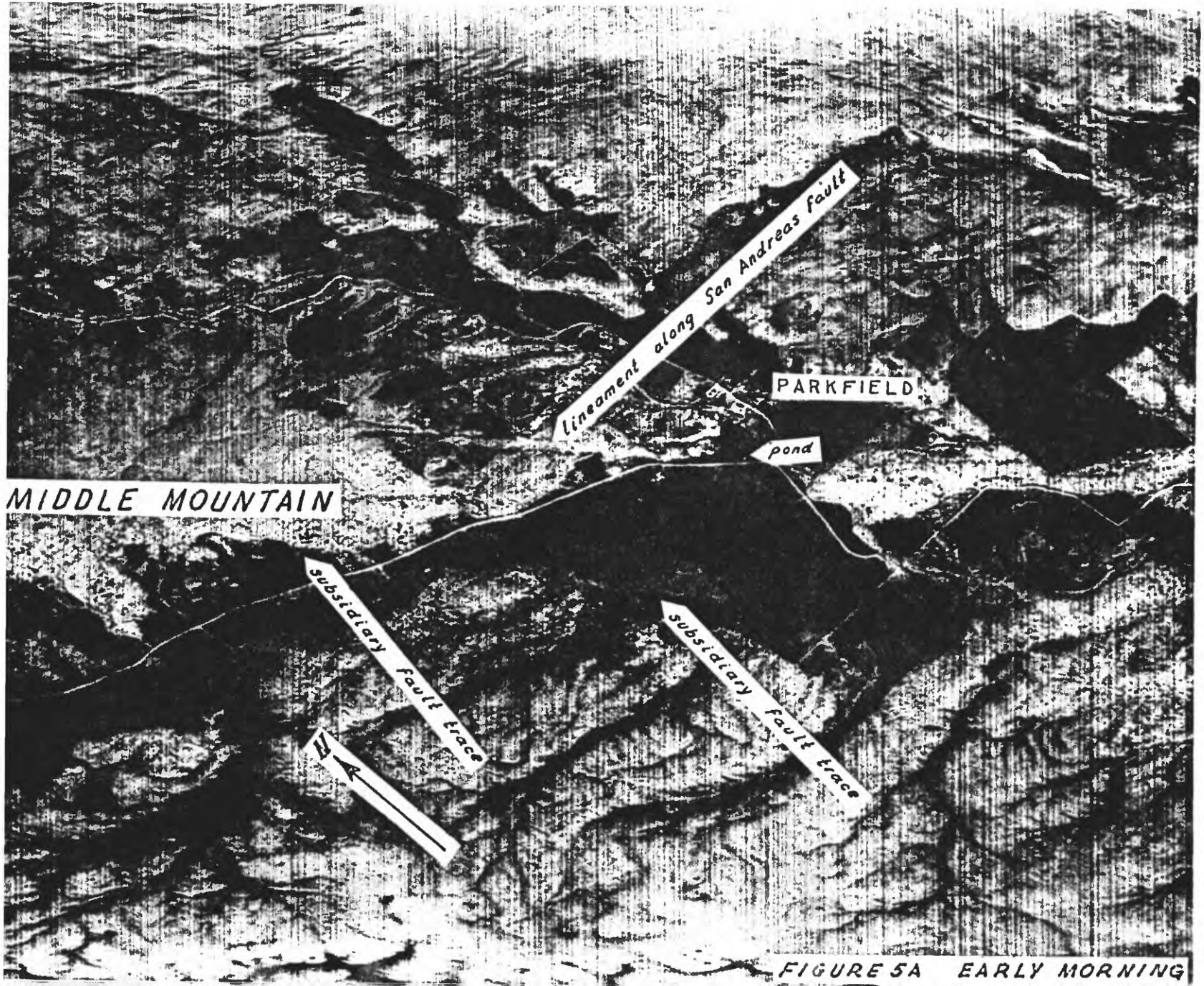

FIGURE 5A EARLY MORNING

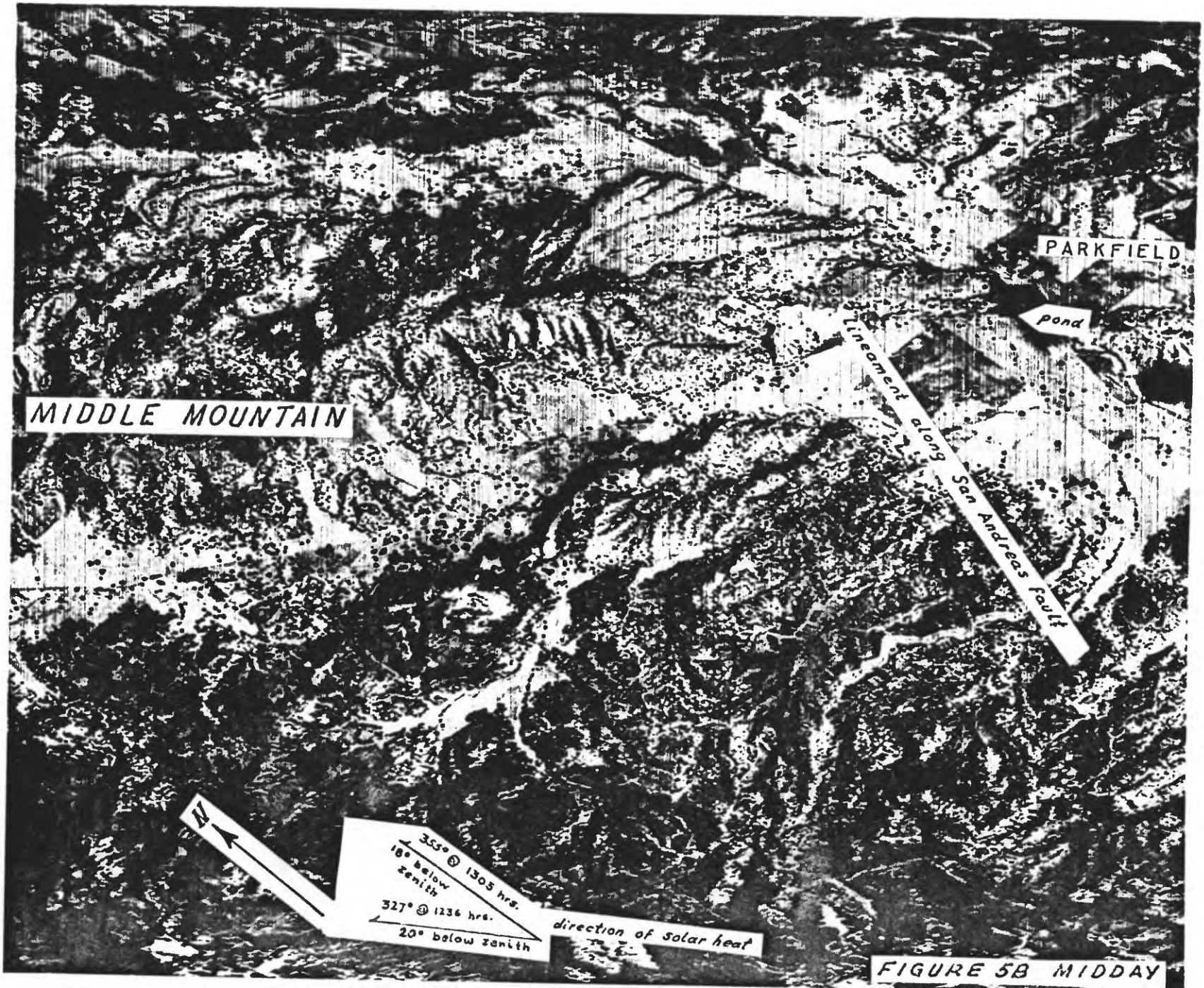

FIGURE 5B MIDDAY

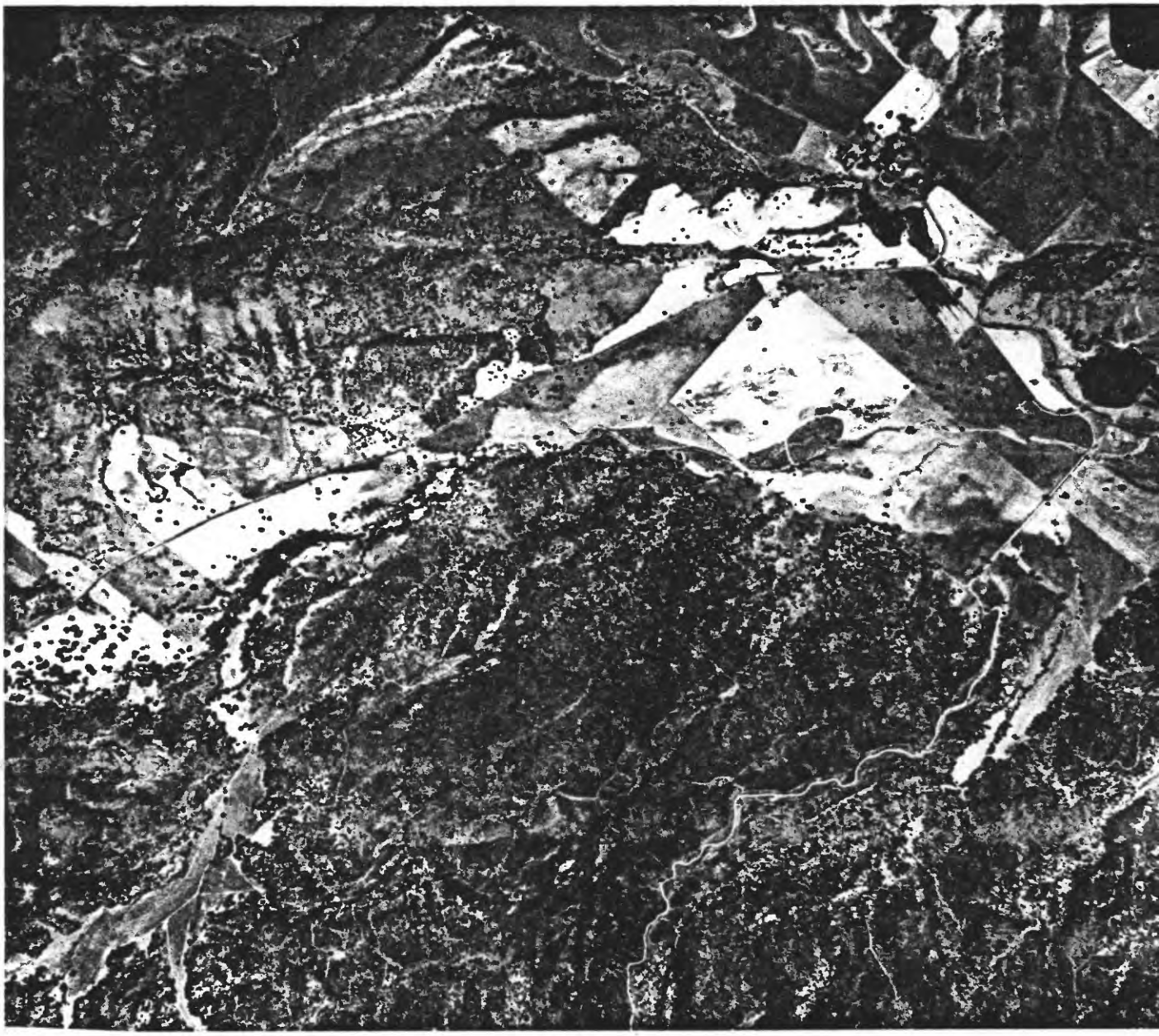

FIGURE 5C PANCHROMATIC

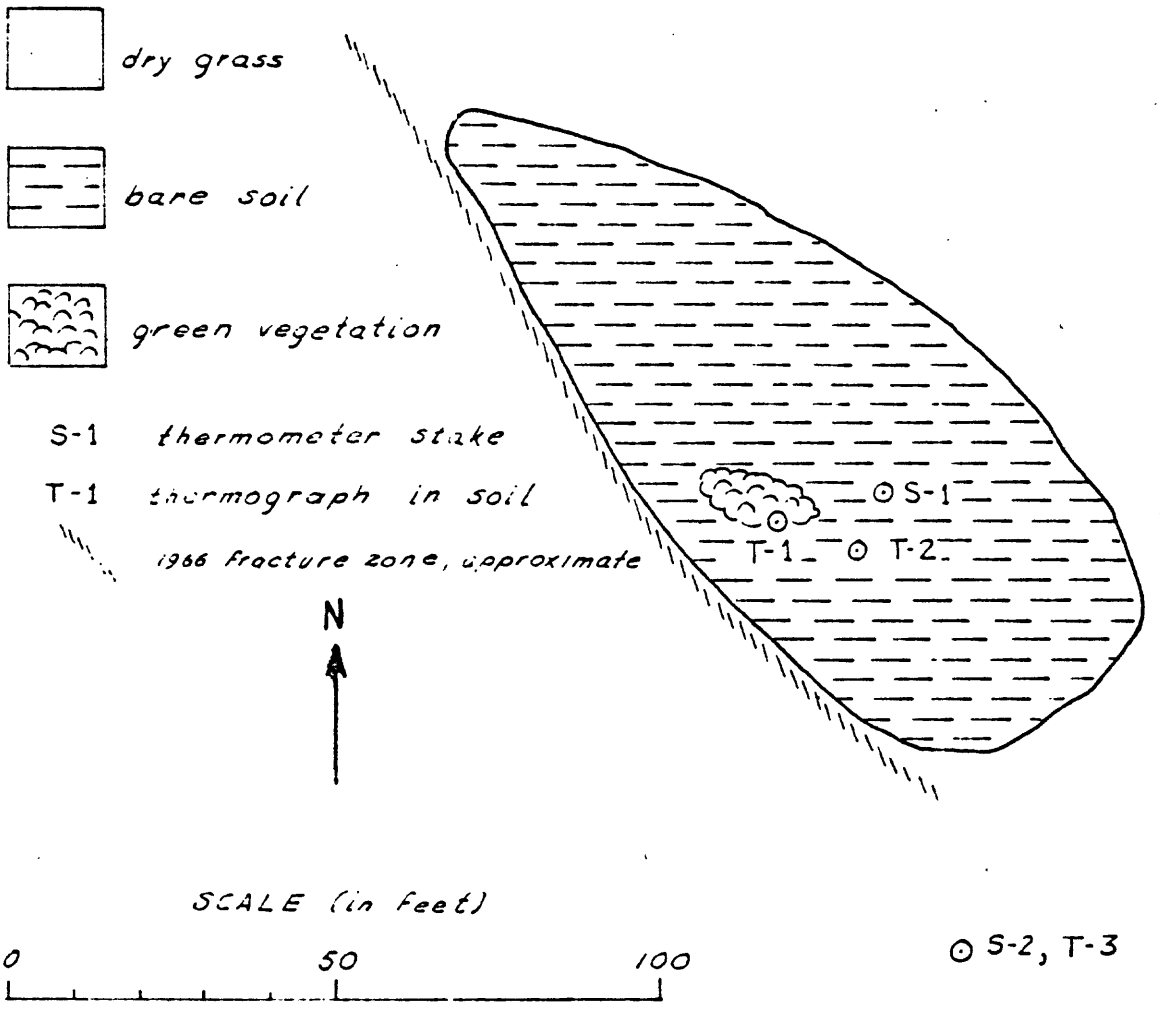

Figure 7.--Sketch map of test area near Gold Hill, site of ground temperature observations of 7-29-68 and 7-30-68.

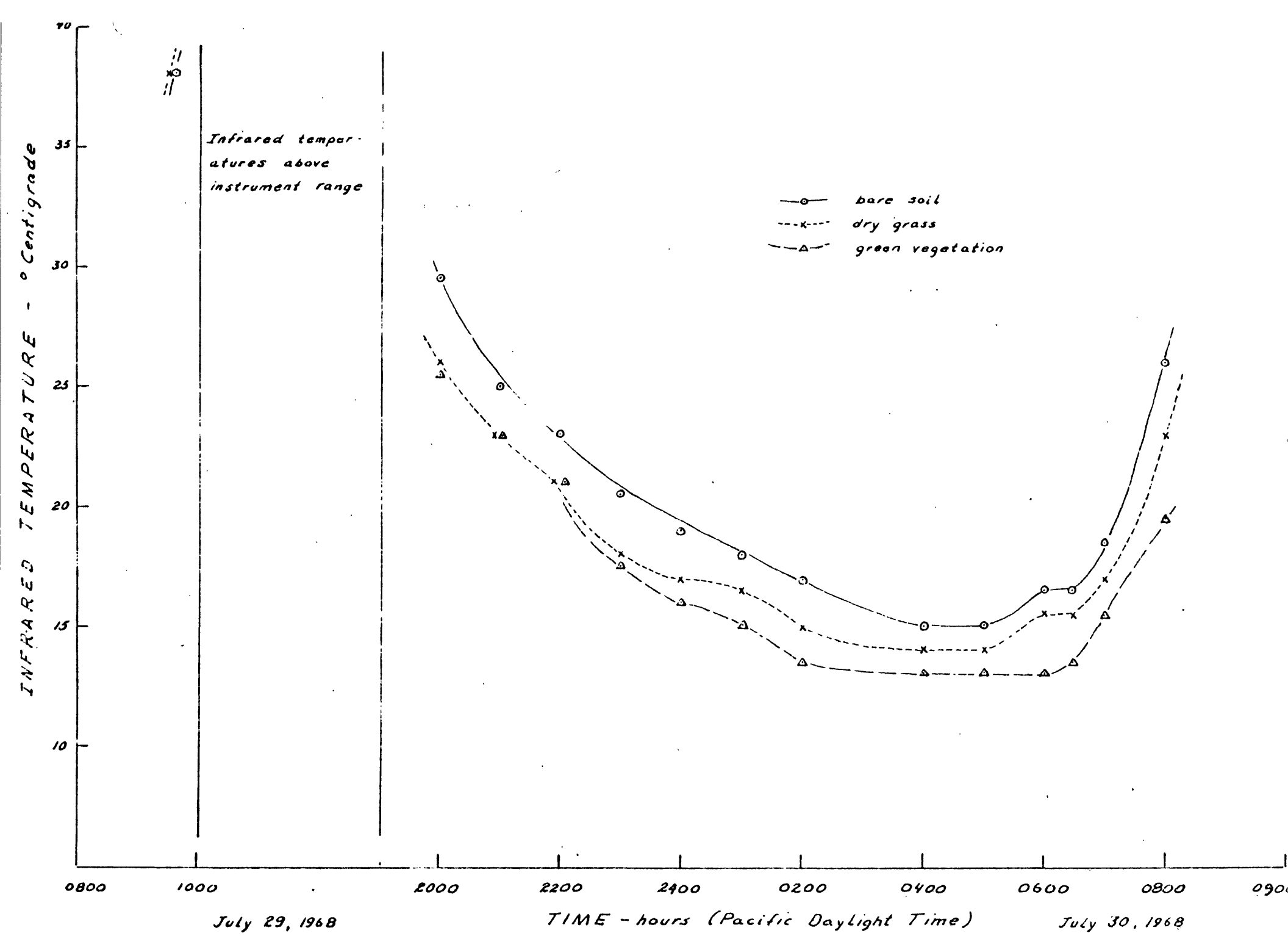

Figure 9.--Comparison of Infrared temperature for bare soil, dry grass, and green vegetation at test area near Gold Hill.